Numerical Analysis of Unsteady Compressor Performance Under Boundary Conditions Caused by Pulsed Detonation Combustion

Nicolai Neumann[1(✉)], Tim Rähse[2], Panagiotis Stathopoulos[2], and Dieter Peitsch[1]

[1] Institute of Aeronautics and Astronautics, Chair for Aero Engines, Technische Universität Berlin, Marchstraße 12–14, 10587 Berlin, Germany
{nicolai.neumann,dieter.peitsch}@tu-berlin.de
[2] Institute of Fluid Dynamics and Technical Acoustics, Chair for Unsteady Thermodynamics in Gas Turbine Processes, Technische Universität Berlin, Müller-Breslau-Straße 8, 10623 Berlin, Germany
{raehse,stathopoulos}@tu-berlin.de

Abstract. Pressure gain combustion is a revolutionary concept to increase gas turbine efficiency and thus potentially reduces the environmental footprint of power generation and aviation. Pressure gain combustion can be realized through pulsed detonation combustion. However, this unsteady combustion process has detrimental effects on adjacent turbomachines. This paper identifies realistic time-variant compressor outlet conditions, which could potentially stem from pulsed detonation combustion. Furthermore, a low fidelity approach based on the 1D-Euler method is applied to investigate the performance of a compressor exposed to these outlet boundary conditions. The simulation results indicate that the efficiency penalty due to unsteady compressor operation remains below 1% point. Furthermore, between 80% and 95% of the fluctuations' amplitudes are damped till the inlet of the 4-stage compressor.

Keywords: Pressure gain combustion · Unsteady 1D-Euler simulation · Compressor performance

Abbreviations and Nomenclature

E^3	Energy efficient engine
PDC	Pulsed detonation combustion
PGC	Pressure gain combustion
A	Cross sectional area
c	Absolute velocity
E	Internal energy
$F_{x,Outlet}$	Outlet surface force
$F_{x,Inlet}$	Inlet surface force

R. King and D. Peitsch (Eds.): AFCC 2021, NNFM 152, pp. 272–287, 2022.
https://doi.org/10.1007/978-3-030-90727-3_17

$F_{x,Endwall}$	Surface force caused by a change in area
$F_{x,Blade}$	Blade force
h	Specific enthalpy
$\dot{m}$	Mass flow
p	Pressure
t	Time
t_{close}	Time during which the combustor is closed
T	Temperature
V_p	Volume of the plenum
W	Work input
$\Delta\Phi$	Relative amplitude of static pressure
ϵ	Unsteady damping
η	Isentropic efficiency
ρ	Density
γ	Ratio of specific heats
$_{ax}$	Quantity in axial direction
$_{in}$	Inlet of component
$_{out}$	Outlet of component
$_{p}$	Quantity in plenum
$_{ma}$	Mass-averaged
$_{wa}$	Work-averaged

1 Introduction

Despite the current pandemic, aviation is seen as an increasing market in the years to come [1,2]. To reduce aviation's emission footprint, the industry committed to the ACARE flightpath 2050, which e.g. aims for a 75% reduction of CO_2 emission compared to a reference aircraft from 2000 [3]. Due to the high energy density requirement both gravimetric and volumetric for long haul flights, which are responsible for 20% of aviation's CO_2 emissions [4], there is currently no alternative to hydrocarbon fuels. Hydrogen appears to be an option for short- and medium-range aircraft when burnt in modified gas turbines [4]. Other propulsion concepts like pure electric or distributed propulsion are still in their infancy and limited to small commuter and regional aircraft. Hence, conventional gas turbine based engines are still indispensable and therefore require further development to meet aforementioned goals. However, the conventional gas turbine engine is a very mature technology, making efficiency improvements increasingly difficult to attain. That is why revolutionary concepts such as pressure gain combustion (PGC) attract a lot of attention. Instead of a constant pressure combustion, which in fact occurs at a pressure loss, the fuel is burned at quasi-constant volume conditions leading to a total pressure increase. In their simplified ideal thermodynamic studies, Heiser and Pratt [5] determined thermal efficiencies of up to 80% using PGC. More recent thermodynamic studies [6,7] also account for reduced turbine efficiency and losses associated with the secondary air system for blade cooling. The PGC cycles, indeed, outpace their Joule counterparts by

up to 10% points in thermal efficiency, especially at low cycle pressure ratios. However, the disadvantage of pressure gain combustion lies in its unsteadiness, which results in time-variant boundary conditions for adjacent turbomachines. Hence, it is very likely that the PGC device will be surrounded by two plena, which dampen the fluctuations. The turbine is most severely affected, when hot gas pressure waves strike onto the turbine blades. That is object of research both experimentally and numerically for several years [8–12]. Less attention is directed towards the compressor, which will be the focus of this paper.

The unsteady periodic combustion leads to a likewise unsteady throttling of the upstream compressor, because the inlet of a combustion tube is closed after ignition, until combustor pressure level allows for refilling. This leads to a mass accumulation in the upstream plenum rising compressor outlet pressure associated with detrimental effects onto compressor performance as the literature survey confirms. Hoke and Bradley [13] connected a turbocharger to two pulsed detonation combustion (PDC) tubes. Even when applying a simultaneous firing pattern, the feasibility could be demonstrated. Sakurai et al. [14] successfully connected two combustion tubes to a radial compressor. One tube operated in PGC mode, whereas the other ran in conventional combustion mode, achieving sustained operation. However, they found cycle performance to be lower compared to full conventional combustion, which they attributed to a decrease in compressor efficiency. When switching the second tube to PGC mode as well, the gas turbine operation could not be sustained. Lu and Zheng [15], in turn, conducted a third experimental study of the PDC-compressor interaction by connecting an arrangement of four PDC tubes to a centrifugal compressor. After examining the sensitivity to the firing pattern and frequency, they concluded that the compressor operates closer to the surge line. At Technische Universität Berlin, various 2D and 3D compressor cascades are exposed to throttling devices that simulate PGC boundary conditions. Active flow control is applied successfully in order to stabilise the flow [16–19].

Numerical studies in this particular field do not always allow a direct comparison. That is due to the way the compressor outlet boundary, which simulates the presence of a PGC device, is specified. Because of the resolution also in circumferential direction, 3D-CFD allows to simulate a sequential firing pattern by a rotating section of elevated pressure. Thus, only part of the compressor outlet domain is throttled. Examples are de Almeida and Peitsch [20–22], who performed 3D-CFD simulations of the rear part of the Rolls Royce E3E and NASA GE E^3 high pressure compressors at varying back pressure frequencies (12%–300% of blade passing frequency) and amplitudes (5%–20%). At low amplitudes, they found the efficiency penalty to be less than 1%, independent of frequency. At high amplitudes, penalties went up to 15%. The authors further claim, that most of the fluctuations are damped across a single stage. Numerical investigations based on a 1D-method usually use boundary conditions with much lower pressure amplitudes. This is because the complete compressor outlet is throttled in 1D. Neumann et al. [23] used a coupled numerical scheme to compute compressor boundary conditions that would result from a PDC device with three

and five combustion tubes. They showed that results of a unsteady quasi 1D-Euler simulation match those computed by 3D-CFD, where also the complete outlet domain is throttled. Furthermore, the efficiency penalty was estimated to be below 1% point for these specific cases and the results suggest that 90% of the fluctuations are damped over the last four stages.

This paper builds upon these findings [23] and substantially extends it by answering the following research questions:

1. What range of compressor boundary conditions can be expected when operated together with a PDC?
2. What is the impact of these boundary conditions onto compressor performance in terms of efficiency? Which part of the compressor is most affected by a certain set of boundary condition?

For that purpose, the paper presents a simplified approach to estimate the amplitude and frequency of pressure fluctuations caused by different plenum volumes and PDC specifications. The results will serve as an input for boundary conditions of 1D-compressor simulations. The compressor performance is evaluated for a wide range of throttle frequencies and amplitudes using a validated 1D-Euler method. In doing so, a comprehensive evaluation of multi-stage compressor performance is presented, which combines the derivation of the compressor boundary conditions and their influence on compressor operation. To the authors' knowledge, no such study has been carried out so far.

2 Method and Compressor Model

The compressor performance is simulated primarily by an unsteady quasi 1D-Euler approach due to its resolution in time and space. However, the momentum and energy equations of the 1D-Euler approach require source terms, in order to account for blade force and work input within the compressor. These source terms are calculated by a mean line method. 1D-Euler and mean line method are briefly introduced next.

The 1D-Euler method was first developed for the simulation of a shockless explosion combustion by Berndt [24] and then extended for the simulation of turbomachines by Dittmar and Stathopoulos [25] and Neumann et al. [23]. For this purpose, the force of the compressor blades ($F_{x,blade}$) and the work of the rotor blades (W_{Rotor}) are integrated into the momentum and energy equations, respectively, as seen in Eq. 1.

$$\frac{\partial}{\partial t}\begin{pmatrix}\rho A\\ \rho c A\\ \rho E A\end{pmatrix}+\frac{\partial}{\partial x}\begin{pmatrix}\rho c A\\ \rho c^2 A+pA\\ cA\left(\rho E+p\right)\end{pmatrix}=\frac{\partial}{\partial x}\begin{pmatrix}0\\ F_{x,Blade}+pA\\ W_{Rotor}\end{pmatrix} \tag{1}$$

The solver uses a second-order finite volume scheme. The inlet conditions are fixed total temperature and total pressure. Static pressure is prescribed at the outlet using a ghost cell. The compressor domain consists of 511 cells each having

a length of 8×10^{-4} m. The mean line method used to compute the source terms in the 1D-Euler equations has been recently developed at the Chair for Aero Engines. A comprehensive introduction is given in [26]. The source terms are computed as follows. The force in axial direction $F_{x,Blade}$ of Eq. 1 is computed from Newton's 2. law of motion.

$$\dot{m} \cdot (c_{x,out} - c_{x,in}) = \sum F_i \tag{2}$$

The sum of forces $\sum F_i$ constitutes of four forces as defined in Eq. 3.

$$\sum F_i = F_{x,Inlet} - F_{x,Outlet} - F_{x,Endwalls} + F_{x,Blade} \tag{3}$$

For a blade row depicted in Fig. 1, $F_{x,Inlet}$ and $F_{x,Outlet}$ act on the inlet and outlet of the control volume with the respective pressure. The mean line method computes entry and exit of a blade row, hence $F_{x,Inlet}$ and $F_{x,Outlet}$. Furthermore, whenever there is a change in area along the x-axis, a force $F_{x,Endwalls}$ acts onto the control volume. Figure 1 depicts this force only a the hub but it could likewise act at the casing. $F_{x,Endwalls}$ is computed by the 1D-Euler code as it is part of the momentum equation (compare right-hand side of Eq. 1). Lastly, there is the blade force $F_{x,Blade}$ in axial direction created by the blades and required for Eq. 1. Combining Eq. 2 with Eq. 3 and solving for $F_{x,Blade}$ gives the required quantity:

$$F_{x,Blade} = \dot{m}(c_{x,out} - c_{x,in}) + F_{x,Outlet} - F_{x,Inlet} + F_{x,Endwalls}, \tag{4}$$

where $F_{x,Outlet} = p_{out} \cdot A_{out}$ and $F_{x,Inlet} = p_{in} \cdot A_{in}$.

The work W_{Rotor} introduced by the rotor blades is calculated from the first law of thermodynamics, Eq. 5. Since the blade row is assumed adiabatic no heat is exchanged.

$$W_{Rotor} = \dot{m}(h_{t,out} - h_{t,in}) \tag{5}$$

The mean line method is executed to compute the source terms for several operating points on a constant speed line of the compressor. The source terms are stored

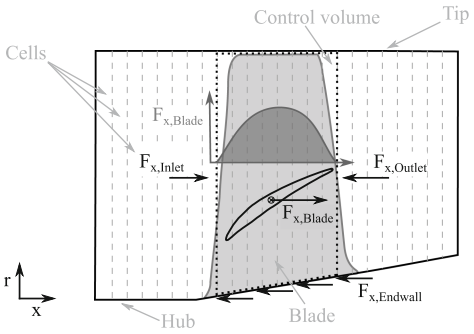

Fig. 1. Sketch of rotor blade with control volume and definition of force source terms, cells size is exaggerated for visibility

in a look-up table, which is used by the 1D-Euler code. Depending on the current axial velocity at the blade leading edge, the 1D-Euler code interpolates the corresponding axial force source term and work source term. These two are distributed among all cells of the blade row in the 1D-Euler code. As sketched in Fig. 1, a parabolic distribution is chosen, which resembles the typical blade loading.

The last four stages of the well-known NASA/GE E^3 high-pressure compressor are modeled for this study [27,28]. The compressor originally consists of ten stages. The analysis is limited to the last four stages starting with rotor 7 because they are mainly affected by the relevant range of boundary conditions. The compressor inlet conditions are selected as if the full ten-stage compressor were operating. The subsequent simulations and analyses use the operating point defined in Table 1.

Table 1. Specifications of the NASA/GE Energy Efficient Engine high pressure compressor operating point of the last four stages

Reduced corrected air mass flow	8.95 kg/s
Pressure ratio	2.36:1
Rotational speed	12669.5 rpm
Inlet total temperature	590.8 K
Inlet total pressure	990.5 kPa
Outlet static pressure	2169 kPa

3 Validation

The compressor model and the presented methods have been validated in a recent publication [23]. Principally, the steady-state results of the mean line method require validation to verify the correctness of the source terms and unsteady results of the 1D-Euler code are compared to results of unsteady 3D-CFD (URANS) to prove the accuracy of the general approach.

3.1 Steady-State Conditions

Results of the steady-state CFD, 1D-Euler and mean line method simulations of the E^3 compressor are compared with published experimental data.

The experimental data of the last four stages is taken from [28] and depicted in Fig. 2. Since the last four stages were not tested separately but always together with the front block of the compressor, throttling at a constant mechanical speed intersects different reduced speed lines on the characteristic as the temperature at the inlet of rotor 7 changes. Hence, experimental data points shown in Fig. 2 are not on a single reduced speed line. Still, the 3D-CFD and the mean line simulations were performed at a constant mechanical speed of 12669.5 rpm and at constant inlet total temperature of 590 K and total pressure of 990 kPa at

rotor 7. These inlet condition were reported in [27] for the predicted design point and selected here, even though they lead to an offset in isentropic efficiency. However, the performance in terms of pressure ratio is captured accurately by 3D-CFD. Since inter blade values of the CFD simulations are used to tune the loss models of the mean line method, also mean line data matches those of the experiment. Regarding isentropic efficiency, mean line results agree with 3D-CFD results but less agreement with experimental data is achieved as explained above. Another shortcoming is that both mean line pressure ratio and isentropic efficiency deviate close to surge from 3D-CFD data. A likely explanation is the assumption of constant flow blockage for all operating points in the mean line simulations. The source terms for the 1D-Euler code will be derived from mean line data of the depicted speed line as outlined in Sect. 2.

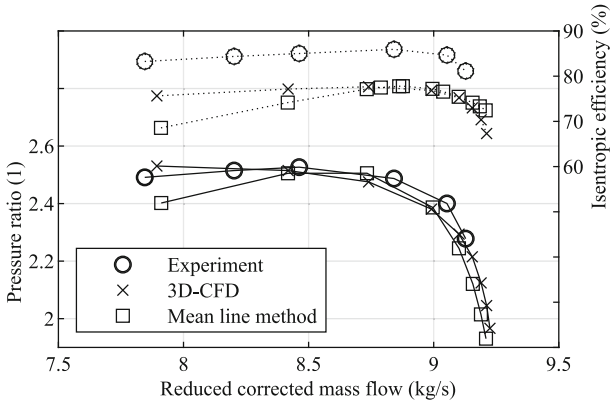

Fig. 2. Comparison of experimental [28], 3D-CFD [23] and mean line method compressor map

3.2 Unsteady Conditions

The unsteady 1D-Euler results are validated against unsteady 3D-CFD results because of their presumably higher fidelity. The complete validation can be found in [23]. Here, only the comparison for a fluctuation with a frequency of 60 Hz and a relative pressure amplitude of 3.6% at the compressor outlet is presented. The relative amplitude is defined in Eq. 6 and is used for the comparison of the results of both numerical methods.

$$\Delta\Phi = \frac{\Phi_{max} - \Phi_{min}}{2 \cdot \Phi_{mean}} \tag{6}$$

$\Delta\Phi$ represents in Eq. 6 the relative amplitude of the periodic variation of static pressure Φ in time. Figure 3 depicts relative amplitudes along the compressor length from 1D-Euler and 3D-CFD simulations. The latter are computed only between rows using a spatial mass flow averaged static pressure. Overall, a

good agreement is found between 1D-Euler and 3D-CFD simulations. 3D-CFD tend to give smaller relative amplitudes which might be explained by viscous effects. They are ignored in the 1D-Euler method between blade rows. In absolute terms, the relative amplitude is reduced for both 3D-CFD and 1D-Euler from 3.6% to 0.3%. Thus, the application of the lower fidelity 1D-Euler method is justified as it gives similar results compared to unsteady 3D-CFD for this representative case.

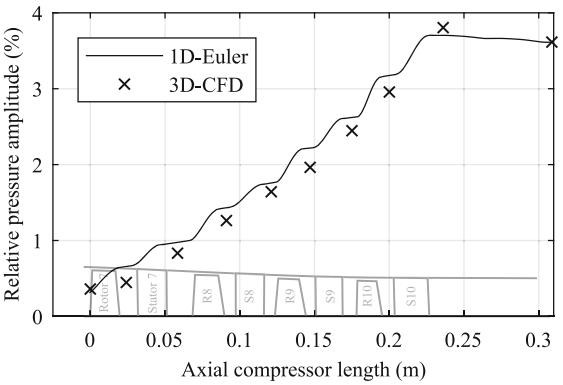

Fig. 3. Comparison of relative pressure amplitude computed by 1D-Euler and 3D-CFD

4 Calculation of Boundary Condition

The 1D-Euler method requires a time-dependent static pressure outlet boundary condition. This outlet pressure simulates the presence of a plenum and PDC tubes downstream of the compressor. Simulations using a 0D-compressor characteristic, 0D-plenum and multiple 1D-PDC tubes show that the resulting pressure trace inside the plenum has a sinusoidal shape [23]. Thus, a compressor outlet boundary condition might be described by a sinusoidal signal of a certain frequency and relative amplitude. In this section realistic ranges for frequencies and relative amplitudes are identified. This is accomplished from two perspectives: Firstly, depending on both the PDC and plenum specifications and state of the fluid, resulting pressure fluctuation are computed. Secondly, maximum tolerable relative amplitudes are identified based on the available surge margin of the compressor using its steady-state map.

The relative amplitude of the pressure fluctuation is derived by an approach by Wintenberger [29]. According to Wintenberger, the relative pressure amplitude can be estimated by Eq. 7.

$$\Delta\Phi = \frac{\dot{m}_0 t_{\text{close}}}{V_P \overline{\rho_P}} \left(\frac{\gamma}{2} + \frac{\gamma - 1}{4} \cdot \frac{\dot{m}_0 t_{\text{close}}}{V_P \overline{\rho_P}} \right) \tag{7}$$

That equations is derived from the unsteady mass and energy equations for a control volume, which comprises the plenum from the compressor exit till the PDC valve plane. This system of equations has been solved separately for the closed part of the cycle and for the open part of the cycle. Details and assumptions used in the derivation can be found in [30]. The amplitude is controlled by a single non-dimensional parameter $\frac{\dot{m}_0 t_{\mathrm{close}}}{V_P \bar{\rho}_P}$, which represents the ratio of the amount of mass added to the plenum during the closed part of the cycle to the average mass in the plenum. In Eq. 7 only the volume of the plenum V_P and t_{close} are variables. $\dot{m}_0$, $\bar{\rho}_P$ and γ are defined by the compressor operating point. t_{close} is defined as the relative closing time divided by the product of firing frequency and number of tubes. The relative closing time is set to 0.05, i.e. the combustion tube is closed during 5% of a firing period. That value is selected as it results in a good match with more complex compressor-plenum-PDC simulations in [23].

The results of Eq. 7 are depicted in Fig. 4, where lines of constant relative amplitude are presented for different frequencies (X-axis) and plenum volumes (Y-axis). The plenum volume is varied between 0.005 m^3–0.1 m^3, which corresponds to 3%–60% of the compressor volume. Frequencies are selected between 20 Hz and 1000 Hz resulting from the literature research for PDCs [31]. The frequency of the sinusoidal wave is a function of the firing frequency of a single tube and the total number of tubes assuming a sequential firing pattern. A firing frequency of 20 Hz is selected for this analysis, since that has been achieved in experiments [32]. Thus, the frequency range between 20 Hz and 1000 Hz corresponds to a number of PDC tubes between 2 and 50. Theoretical approaches such as in [33] tend to suggest higher firing frequencies in the order of 200 Hz. This is a result of the assumption of a completely formed detonation once the fuel air mixture ignites. In reality, a deflagration to detonation transition is required, which reduces wave velocity and results in lower cycle frequencies.

Three main observations can be made from Fig. 4:

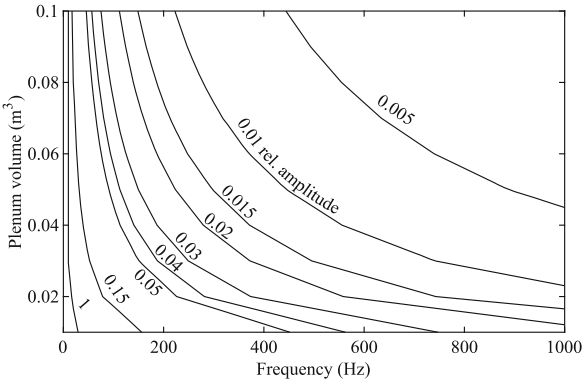

Fig. 4. Isolines of constant relative amplitude for varying frequencies and plenum volumes

- At high plenum volumes and low frequencies (top left), relative amplitudes are very sensitive to frequency but little to plenum volume. Even a small increase in frequency substantially reduces relative amplitude.
- Vice versa is true at high frequencies and low plenum volumes. Relative amplitude is very sensitive to plenum volume but little sensitive to frequency. Here, even a small increase in plenum volume significantly reduces the relative amplitude.
- Around an imaginary diagonal line on the plot, increasing both plenum volume and frequency results in lower relative amplitudes.

According to Fig. 4, relative amplitudes reach values as high as their mean value (relative amplitude = 1). Obviously, that is intolerable from a compressor stability perspective. Therefore, a maximum permissible relative amplitude is inferred from the compressor map, which is a simplification, since the compressor map depicts steady-state operation. The time-averaged operating point is positioned at a pressure ratio of 2.36 for this study, which is below the intended design point of the compressor. However, that operating point allows for relative amplitudes of 5% without exceeding the surge line on the steady-state map and eve provides some safety margin. As a result, the compressor model will be simulated under boundary conditions with frequencies in the range of 50 Hz–1000 Hz and amplitudes between 0.5%–5% around a mean static outlet pressure of 2169 kPa, which corresponds to a pressure ratio of 2.36 of the last four stages.

5 Compressor Simulation Results

Previously identified boundary conditions were simulated for the operating point defined in Table 1. The simulations were run for multiple periods to allow for an unsteady periodic convergence. Eventually, convergence was verified by a method, which relies on fundamental concepts from digital signal processing including the discrete Fourier transform and cross correlation [34].

5.1 Unsteady Damping

Any excitation is damped in a viscous and compressible medium. In case of a compressor exposed to a fluctuating outlet pressure profile, the pressure waves lose strength and eventually vanish while travelling upstream. This rate of dissipation is quantified by the unsteady damping ϵ of the relative amplitude (compare Eq. 6).

$$\epsilon = \frac{\Delta\Phi_2 - \Delta\Phi_1}{\Delta\Phi_2} \tag{8}$$

$\Delta\Phi_2$ is the relative amplitude at the compressor exit and $\Delta\Phi_1$ is located arbitrarily further upstream.

Unsteady damping is plotted over frequency and relative amplitude. By evaluating different planes within the compressor, the damping characteristic can be inferred. Figure 5 depicts unsteady damping at the inlet of the last stage and Fig. 6 shows unsteady damping upstream of the first rotor.

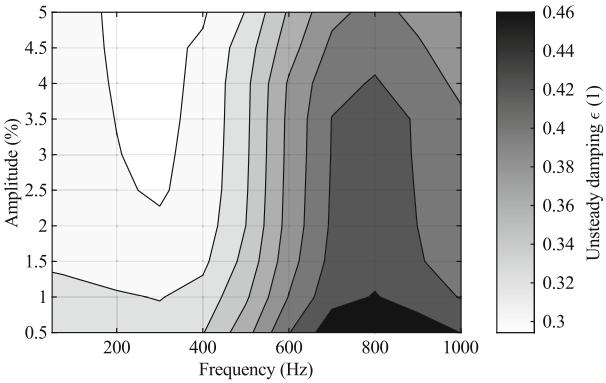

Fig. 5. Unsteady damping at the inlet of the last stage

White areas indicate less damping whereas black stands for a higher degree of damping. From Fig. 5 is can be inferred that low frequencies are less damped than high frequencies. According to the data, roughly 30% of the fluctuation's pressure amplitude is attenuated at 200 Hz whereas 46% are damped at 800 Hz. Furthermore, the results suggest that relative amplitude does not have a strong effect on unsteady damping. That is especially true for frequencies between 400 Hz–700 Hz.

Taking into account Fig. 6, which depicts unsteady damping taken at the inlet, a different picture is drawn. Low frequencies are more damped than high frequencies. Frequencies below 200 Hz have an unsteady damping of as high as 94%, whereas only 82% of the outlet fluctuation is attenuated at high frequencies. It can be concluded that fluctuations with a high frequency show a high amount of damping within the last stage, but as soon as their amplitudes are lower the rate of damping reduces. Hence, at the inlet higher relative amplitudes are observed for fluctuations with a high frequency compared to a fluctuation with a low frequency.

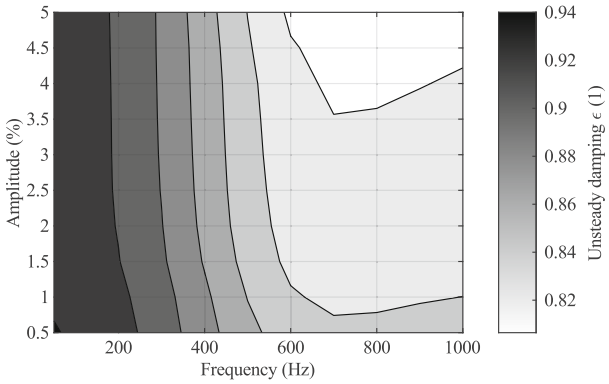

Fig. 6. Unsteady damping at the inlet of the four-stage compressor

5.2 Isentropic Efficiency

Next, compressor isentropic efficiency is presented for the range of selected boundary conditions. Isentropic efficiency is a suitable metric as it relates the ideal energy input with the real energy input required to achieve a certain pressure ratio. The definition is given in Eq. 9.

$$\eta_{is} = \frac{\Delta h_{ideal}}{\Delta h_{real}} = \frac{(p_{t,out}/p_{t,in})^{\overline{\gamma}/(\overline{\gamma}-1)} - 1}{T_{t,out}/T_{t,in} - 1} \tag{9}$$

Temperatures and pressure are averaged to obtain a representative value for a complete firing period. For that, an averaging procedure presented by [35] and successfully applied in [10,23] to calculate isentropic efficiency will be used. Instead of using instantaneous values in Eq. 9 to yield a time resolved efficiency, temperatures are mass-averaged and pressures are work-averaged over one period. A mass-averaged temperature is computed by Eq. 10 for both inlet and outlet:

$$T_t{}^{ma} = \frac{\int_{t_1}^{t_2} \rho c T_t d\xi}{\int_{t_1}^{t_2} \rho c d\xi} \tag{10}$$

The work-averaged pressures at inlet and outlet are averaged differently according to [35]. Work-averaged total inlet pressure is defined as:

$$\left(p_{t,in}^{\mathrm{wa}}\right)^{(\gamma-1)/\gamma} = \frac{\int_{t_1}^{t_2} \rho_{in} c_{in} T_{t,in}(\xi) d\xi}{\int_{t_1}^{t_2} \rho_{in} c_{in} \left(\frac{T_{t,in}(\xi)}{p_{t,in}(\xi)^{(\gamma-1)/\gamma}}\right) d\xi} \tag{11}$$

and work-averaged outlet pressure as:

$$\left(p_{t,out}^{\mathrm{wa}}\right)^{(\gamma-1)/\gamma} = \frac{1}{\Delta t} \int_{t_1}^{t_2} p_{t,out}^{(\gamma-1)/\gamma}(\xi) d\xi. \tag{12}$$

The mass and work-averaged definition for isentropic efficiency has the advantage that the assumption of an instantaneous compression through the compressor is not required [35].

Again, data is depicted over relative amplitude and frequency in Fig. 7. The isentropic efficiency is presented as delta efficiency. That is the difference between a steady-state efficiency of an operating point having the same minimum surge margin as the unsteady throttled operation. It can be inferred that isentropic efficiency penalties remain below 1% point for the selected boundary conditions. The efficiency penalty is dominantly influenced by relative amplitude. The frequency of the boundary condition does not have a strong effect on efficiency. At low relative amplitudes, isentropic efficiency is only penalized by 0.1% point. At high relative amplitudes of 5%, efficiency penalties amount to 1% point. For every percentage point increase in relative amplitude, the efficiency penalty is increases by roughly 0.2% point. The penalty can be decreased by going for a lower relative amplitude of the boundary condition. That can be achieved by a larger plenum, as Fig. 4 suggests.

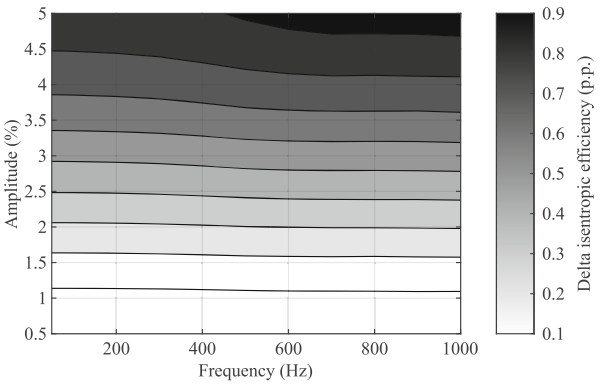

Fig. 7. Isentropic efficiency penalty caused by unsteady boundary condition

6 Conclusion

This paper presents the application of a low fidelity numerical method, in order to investigate compressor behaviour at unsteady boundary conditions similar to those caused by pulsed detonation combustion. For this purpose, a range of reasonable unsteady compressor boundary conditions is derived for different pulsed detonation combustion specifications and plenum sizes. That time-variant static pressure trace is further prescribed at the outlet of a 4-stage compressor model. A fast quasi 1D-Euler method simulates the compressor performance for multiple periods. The results are evaluated with regards to unsteady damping and isentropic efficiency. The main conclusions are:

- relative amplitude and frequency range from 0.5%–5% and 50 Hz–1000 Hz, respectively, for a realistic pulsed detonation combustor and the underlying 1D-approach according to the simplified model.
- The unsteady damping depends on fluctuation frequencies. The last stage dampens between 30%–46% of the fluctuation's amplitude. Between 84% and 92% are attenuated till the inlet of the 4-stage compressor model.
- Compressor isentropic efficiency is influenced by the relative amplitude of the fluctuations. A penalty due to unsteady operation of up to 1% point compared to a comparable steady-state operating point is observed.

The penalty in compressor efficiency is minor, which is likely specific to this compressor, as the modelled compressor does not suffer from a strong decrease in efficiency when moving closer to the surge line (compare Fig. 2). However, the authors believe that the fluctuations' amplitudes are more restricted by stability concerns than by the expected penalty on compressor efficiency. Especially as the last stages are critical in terms of stability at high reduced speeds encountered at a possible cruise operating point. Further research using the presented method is in order that adequately evaluates the influence of pressure gain combustion on compressor stability.

Acknowledgement. Funding: The authors gratefully acknowledge the support by the Deutsche For-schungsgemeinschaft (DFG) as part of the Collaborative Research Center SFB 1029 "Substantial efficiency increase in gas turbines through direct use of coupled unsteady combustion and flow dynamics" in project D01.

References

1. International Civil Aviation Organization - ICAO: Annual report of the council, May 2018
2. International Air Transport Association - IATA: 20 year passenger forecast, 2020
3. Krein, A., Williams, G.: Flightpath 2050: Europe's vision for aeronautics. In: Innovation for Sustainable Aviation in a Global Environment: Proceedings of the Sixth European Aeronautics Days, p. 63 (2012). https://doi.org/10.2777/50266
4. Fuel Cell and Hydrogen Joint Undertaking: Hydrogen powered aviation: a fact-based study of hydrogen technology, economics, and climate impact by 2050 (2020)
5. Heiser, W.H., Pratt, D.T.: Thermodynamic cycle analysis of pulse detonation engines. J. Propul. Power **18**(1), 68–76 (2002). https://doi.org/10.2514/2.5899
6. Neumann, N., Woelki, D., Peitsch, D.: A comparison of steady-state models for pressure gain combustion in gas turbine performance simulation. In: Proceedings of GPPS Beijing 2019, Beijing, China, 16–18 September 2019 (2019)
7. Stathopoulos, P.: Comprehensive thermodynamic analysis of the humphrey cycle for gas turbines with pressure gain combustion. Energies **11**(12), 3521 (2018). https://doi.org/10.3390/en11123521
8. Glaser, A.J., Caldwell, N., Gutmark, E.: Performance measurements of a pulse detonation combustor array integrated with an axial flow turbine. In: 44th AIAA Aerospace Sciences Meeting and Exhibit, pp. 1–12, January 2006. https://doi.org/10.2514/6.2006-1232

9. Schliwka, T., Tiedemann, C., Peitsch, D.: Interaction of main flow and sealing air across a turbine cavity under unsteady conditions. In: ISABE - 22th International Symposium on Air Breathing Engines, Phoenix, Arizona, USA, October 2015. ISABE-2015-21288
10. Xisto, C., Petit, O., Grönstedt, T., Rolt, A., Lundbladh, A., Paniagua, G.: The efficiency of a pulsed detonation combustor-axial turbine integration. Aerosp. Sci. Technol. **82–83**, 80–91 (2018). https://doi.org/10.1016/j.ast.2018.08.038. ISSN: 1270-9638
11. Heinrich, A., Herbig, M., Peitsch, D., Topalovic, D., King, R.: A testrig to evaluate turbine performance and operational strategies under pulsating inflow conditions. In: AIAA - Propulsion and Energy 2019 Forum, Indianapolis, Indiana, USA. American Institute of Aeronautics and Astronautics, August 2019. Ch. AIAA 2019-4039, ISBN: 978-1-62410-590-6. https://doi.org/10.2514/6.2019-4039
12. Liu, Z., Braun, J., Paniagua, G.: Integration of a transonic highpressure turbine with a rotating detonation combustor and a diffuser. Int. J. Turbo Jet-Engines (2020). ISSN: 0020-7403. https://doi.org/10.1515/tjeng-2020-0016
13. Hoke, J., Bradley, R., Stutrud, J., Schauer, F.: Integration of a pulsed detonation engine with an ejector pump and with a turbo-charger as methods to self-aspirate. In: 40th AIAA Aerospace Sciences Meeting & Exhibit, Reno, USA, p. 615 (2002). https://doi.org/10.2514/6.2002-615
14. Sakurai, T., Nakamura, S.: Performance and operating characteristics of micro gas turbine driven by pulse, pressure gain combustor. In: Proceedings of the ASME Turbo Expo 2020: Turbomachinery Technical Conference and Exposition, 21–25 September 2020 (2020). https://doi.org/10.1115/GT2020-15000
15. Lu, J., Zheng, L., Wang, Z., Wang, L., Yan, C.: Experimental investigation on interactions between a two-phase multi-tube pulse detonation combustor and a centrifugal compressor. Appl. Therm. Eng. **113**, 426–434 (2017). https://doi.org/10.1016/j.applthermaleng.2016.10.188
16. Staats, M., Nitsche, W.: Experimental investigations on the efficiency of active flow control in a compressor cascade with periodic non-steady outow conditions In: Volume 2A: Turbomachinery. American Society of Mechanical Engineers, June 2017. https://doi.org/10.1115/gt2017-63246
17. Brück, C., Mihalyovics, J., Peitsch, D.: Experimental investigations on highly loaded compressor airfoils with different active ow control parameters under unsteady ow conditions. In: Proceedings of GPPS Montreal, Montreal, Canada, May 2018. GPPS-2018-0054. https://doi.org/10.5281/zenodo.1343489
18. Werder, T., Liebich, R., Neuhäuser, K., Behnsen, C., King, R.: Active flow control utilizing an adaptive blade geometry and an extremum seeking algorithm at periodically transient boundary conditions. J. Turbomach. **143**(2) (2020). ISSN: 0889-504X. https://doi.org/10.1115/1.4049787
19. Fietzke, B., Mihalyovics, J., King, R., Peitsch, D.: Binary repetitive model predictive active flow control applied to an annular compressor stator cascade with periodic disturbances. In: Proceedings of the ASME Turbo Expo 2021: Turbomachinery Technical Conference and Exposition, 07–11 June 2021. American Society of Mechanical Engineers (2021). GT2021-58 744
20. de Almeida, V.B.C., Peitsch, D.: Aeroelastic assessment of a highly loaded high pressure compressor exposed to pressure gain combustion disturbances. J. Glob. Power Propul. Soc. **2**, 477–492 (2018). https://doi.org/10.22261/jgpps.f72ouu
21. de Almeida, V.B.C., Peitsch, D.: Multirow performance and aeroelastic analyses of a compressor subjected to disturbances from pressure gain combustion. In: Proceedings of the 15th ISUAAAT, Oxford, UK, September 2018. ISUAAAT15-031

22. de Almeida, V.B.C., Motta, V., Peitsch, D.: Unsteady aerodynamics of a high pressure compressor working under pressure gain combustion disturbances. In: IGTC - International Gas Turbine Congress, Tokyo, Japan, November 2019. IGTC2019-0070. http://igtc2019.org/IGTC19_ContentListWeb_4.html/#wepm14_01
23. Neumann, N., Asli, M., Garan, N., Peitsch, D., Stathopoulos, P.: A fast approach for unsteady compressor performance simulation under boundary condition caused by pressure gain combustion. Appl. Therm. Eng. **196**, 117223 (2021). https://doi.org/10.1016/j.applthermaleng.2021.117223. ISSN: 1359-4311
24. Berndt, P., Klein, R., Paschereit, C.O.: A kinetics model for the shockless explosion combustion. In: Turbo Expo: Power for Land, Sea, and Air, vol. 49767. American Society of Mechanical Engineers (2016). V04BT04A034
25. Dittmar, L., Stathopoulos, P.: Numerical analysis of the stability and operation of an axial compressor connected to an array of pulsed detonation combustors. In: Proceedings of the ASME Turbo Expo 2020: Turbomachinery Technical Conference and Exposition, 21–25 September 2020. American Society of Mechanical Engineers (2020)
26. Neumann, N., Peitsch, D.: Introduction and validation of a mean line solver for present and future turbomachines. In: Proceedings of ISABE, Canberra, Australia, 22–26 September 2019 (2019). ISABE-2019-24441
27. Holloway, P., Koch, C., Knight, G., Shaffer, S.: Energy efficient engine - high pressure compressor detail design report (1982). NASA-CR-165558
28. Cline, S., Fesler, W., Liu, H., Lovell, R., Shaffer, S.: High pressure compressor component performance report (1983). NASA-CR-168245
29. Wintenberger, E., Shepherd, J.E.: Thermodynamic cycle analysis for propagating detonations. J. Propul. Power **22**(3), 694–698 (2006). https://doi.org/10.2514/1.12775
30. Wintenberger, E.: Application of steady and unsteady detonation waves to propulsion. Ph.D. thesis, California Institute of Technology (2004)
31. Perkins, H.D., Paxson, D.E.: Summary of pressure gain combustion research at NASA, April 2018. NASA TM-2018-219874
32. Völzke, F.E., Yücel, F.C., Gray, J.A.T., Hanraths, N., Paschereit, C.O., Moeck, J.P.: The influence of the initial temperature on DDT characteristics in a valveless PDC. In: King, R. (ed.) Active Flow and Combustion Control 2018. NNFMMD, vol. 141, pp. 185–196. Springer, Cham (2019). https://doi.org/10.1007/978-3-319-98177-2_12 ISBN: 978-3-319-98177-2
33. Mitrofanov, V., Zhdan, S.: Thrust performance of an ideal pulse detonation engine. Combust. Explos. Shock Waves **40**(4), 380–385 (2004). https://doi.org/10.1023/B:CESW.0000033559.75292.8e
34. Clark, J.P., Grover, E.A.: Assessing convergence in predictions of periodic-unsteady flowfields. J. Turbomach. **129**(4), 740–749 (2006). https://doi.org/10.1115/1.2720504
35. Suresh, A., Hofer, D.C., Tangirala, V.E.: Turbine efficiency for unsteady, periodic flows. J. Turbomach. **134**(3) (2011). https://doi.org/10.1115/1.4003246